Vibrational Excitation Mechanisms in Electron Energy Loss Spectroscopy Studies of Hydrogen Adsorbed on Si(100) and Ge(100)

J. Eggeling, G. R. Bell, and T. S. Jones*

Department of Chemistry and Centre for Electronic Materials and Devices, Imperial College of Science, Technology and Medicine, London SW7 2AY, U.K.

Received: June 29, 1999; In Final Form: August 30, 1999

High-resolution electron energy loss spectroscopy (HREELS) has been used to investigate the inelastic electron scattering processes involved in the excitation of the normal modes of vibration of atomic hydrogen adsorbed on Si(100) and Ge(100). Detailed measurements as a function of incident electron beam energy allow a clear distinction to be made between dipole and nondipole excitation processes. The bending and scissor modes of adsorbed hydrogen are excited predominantly by dipole scattering, but the stretching modes show characteristic resonances between 3 and 6 eV. The mechanism for these scattering processes is discussed.

1. Introduction

The inelastic scattering of low-energy electrons (<30 eV) from adsorbates is a complex phenomenon that can generally be divided into two categories, dipole and nondipole excitation.[1−4] Dipole scattering involves vibrational excitation by absorption of an energy quantum from the electric field associated with the incoming (or outgoing) electrons. The interaction is long range, and the momentum transfer is very small. In the case of an ordered adsorbate overlayer, forward scattering dominates and the electrons appear in a narrow lobe close to the specular (or Bragg diffraction) direction. For adsorption on a metal surface, the rapid response of the conduction electrons to the approaching electron means that only vibrational modes having a dipole component normal to the surface are excited. More generally, dielectric theory predicts that the intensity of a vibrational mode normal to the surface with respect to parallel modes depends on the square of the substrate dielectric constant.[1] The dipole selection rule is therefore valid for adsorption on both metals and semiconductors, since this value typically exceeds 100.

Nondipole scattering processes are more complex, and there are two processes that have been identified, impact and resonance scattering.[1−4] Impact scattering is a short-range interaction involving direct scattering off the ion cores of the adsorbate/substrate complex. Electron scattering occurs over a wide range of solid angles and the cross section is generally larger for high incident electron energies. Theoretical treatments are more complex than for dipole excitation and require a microscopic consideration of the electron−molecule interaction.[5−8]

Resonance scattering is another short-range interaction that involves capture of the incident electrons at certain beam energies, either by the surface (a surface resonance, SR) or the adsorbate (a negative ion resonance, NIR).[1−4] In the case of NIR, this generally involves an orbital of antibonding character and leads to the formation of a negative ion state with an extended equilibrium internuclear separation relative to that of the ground state molecule. The molecule is therefore left in a vibrationally excited state once the electron escapes. This process is well-known in the gas phase[9] and has become a more commonly observed phenomenon in HREELS studies of adsorbates, both physisorbed and chemisorbed.[10−20] It is characterized by a strong enhancement in the intensity of selective vibrational modes over a narrow incident electron energy range, often accompanied by significant overtone intensity. Since certain symmetry-based selection rules have also been established for this excitation mechanism,[13,14] and the preferred direction of electron capture and emission is a function of the symmetry of the orbital, predictions can be made for the molecular orientation and geometric structure.[10,18−20] The crystal surface can also play an important role by temporarily trapping the electron in surface states at energies above the vacuum level (SR).[21] This occurs when the kinetic energy of the electron normal to the surface is insufficient to overcome the potential barrier produced by the electron/substrate interaction, causing sustained multiple scattering between the barrier and the crystal. These temporary states are quantized and expected just below the emergence of Bragg beams out of the surface. Strong variations in the elastic intensity are expected, and since the lifetime of these states is relatively long, resonant enhancements of inelastic vibrational losses may occur.[22−24]

The different experimental characteristics of each scattering process allow identification of a specific mechanism by monitoring the energy and angular dependence of the vibrational loss intensity.[1−4,25] Furthermore, the distinction between dipole and nondipole excitation is also possible since theoretical predictions for energy and angular distributions assuming dipole scattering behavior are relatively straightforward[26,27] and have been shown to be accurate for the case of ordered adsorbates on metal surfaces.[28,29] By contrast, there have been very few HREELS studies of adsorbates on semiconductor surfaces with the specific aim of identifying the different vibrational excitation processes. In this paper, we present such a study for two archetypal adsorbate systems, namely atomic hydrogen adsorbed on Si(100) and Ge(100). These systems were chosen for three basic reasons: (i) they have been well characterized using a wide range of techniques including HREELS;[30−39] (ii) they exhibit a number of well ordered phases; (iii) the vibrational spectra for each phase are relatively simple to interpret since only a few vibrational modes are present.

* Corresponding author. Phone: +44-171-594-5794. Fax: +44-171-594-5801. E-mail: t.jones@ic.ac.uk.

10.1021/jp992217p CCC: $18.00
Published on Web 10/07/1999

2. Experimental Section

The experiments were performed in an ultrahigh vacuum (UHV) system (base pressure $<3 \times 10^{-10}$ mbar) equipped with HREELS and LEED. The HREEL spectrometer (HIB1000) consists of a double pass cylindrical rotatable monochromator and a fixed analyzer assembly.[40] The Si(100) (p-type, B-doped, $n \approx 1 \times 10^{16}$ cm^{-3}) and Ge(100) (n-type, Sb-doped, $n \approx 1 \times 10^{14}$ cm^{-3}) substrates were initially cleaned in situ by annealing the samples at 900 and 600 K, respectively. This was followed by cycles of argon ion bombardment (800 eV, 3 μA for Si; 600 eV, 2 μA for Si) and annealing (950 K for Si, 800 K for Ge), before a final rapid anneal at 1400 K for Si and 900 K for Ge. Annealing was performed by electron bombardment, and the temperature was monitored using a chromel−alumel thermocouple that was calibrated using a pyrometer. These cleaning procedures resulted in well-ordered surfaces exhibiting sharp (2×1) and (1×2) domains in LEED. Surface contamination was checked by HREELS. It was not possible to fully remove water contamination from the Si(100) surface, and the HREELS spectra showed losses at 800 cm^{-1} (Si−OH stretching and bending vibrations) and 3700 cm^{-1} (O−H stretching vibration).[41] No such losses were observed on the Ge(100) surface, consistent with its lower reactivity.[42] Atomic hydrogen was produced via cracking at a hot tungsten filament placed approximately 5 cm away from the sample. All exposures are given in Langmuirs (1 L = 1×10^{-6} Torr s) of molecular hydrogen.

Energy-dependent HREELS measurements were carried out in specular scattering geometry ($\alpha_i = 45°$, $\alpha_s = 45°$) over a range of incident electron beam energies (1 eV $< E_0 <$ 60 eV). Off-specular measurements involved rotation of the monochromator at a fixed E_0. The resolution of the spectrometer (fwhm) in the "straight-through" position was 20−24 cm^{-1}, while a resolution of approximately 80 cm^{-1} was obtained from the clean Si(100) surface. There was a significant temperature dependence in the width of the elastic peak in the HREEL spectra recorded from the H/Ge(100) surface. A fwhm of ∼150 cm^{-1} was observed at room temperature, but this was reduced to 40 cm^{-1} at 200 K. This broadening is due to the thermal excitation of free carriers and will be the subject of a further publication.

3. Results and Discussion

3.1. Adsorbate Characterization. A full characterization of the adsorbate systems was performed prior to detailed investigation of the vibrational excitation mechanisms. The assignment of vibrational features and the general coverage and temperature-dependent behavior of the adsorption of H on Si(100) and Ge(100) is consistent with previous HREELS studies,[32,37] and only a brief summary is presented in this section.

Initial exposure of the Si(100) surface to hydrogen (<100 L) leads to the development of a Si−H bending mode, ω(SiH), at 625 cm^{-1} and a Si−H stretching mode, ν(SiH), at 2095 cm^{-1}, respectively, indicating the establishment of the monohydride phase via saturation of the dangling bonds (Figure 1). The LEED pattern is consistent with two orthogonal (2×1) domains, its increased sharpness compared to the clean surface suggesting dimer and back-bond relaxation due to saturation of the dangling bonds. Higher exposures (>100 L) result in the appearance of a scissor (deformation) mode ($\delta(SiH_2)$) at 905 cm^{-1}, and a shift in the frequency of the bending ($\omega(SiH_2)$) and stretching ($\nu(SiH_2)$) modes to 635 and 2105 cm^{-1}, respectively, a process which is complete for exposures above ∼600 L (Figure 1). The corresponding LEED pattern indicated a slow transition to a

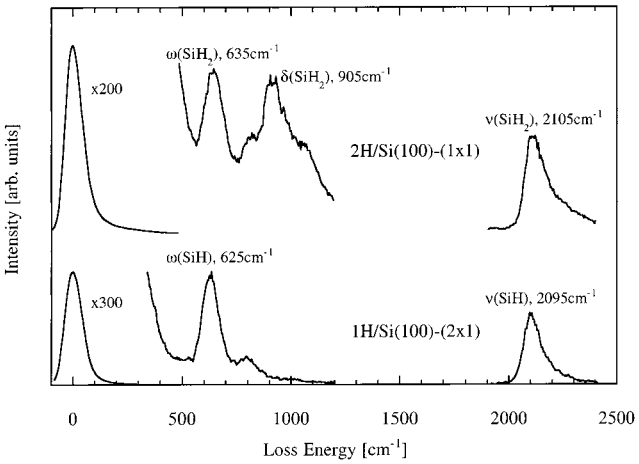

Figure 1. Specular ($\alpha_i = \alpha_s = 45°$) HREELS spectra of the monohydride (1H/Si(100)−(2×1)) and dihydride (2H/Si(100)−(1×1)) phases of atomic H adsorbed on Si(100). The incident electron energy was 4 eV in both cases.

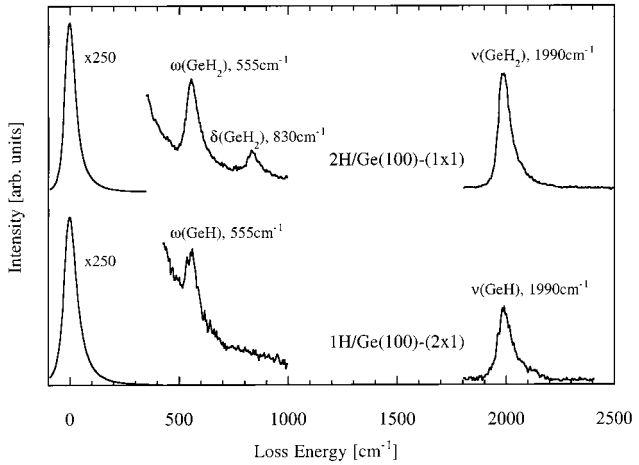

Figure 2. Specular ($\alpha_i = \alpha_s = 45°$) HREELS spectra of the monohydride (1H/Ge(100)−(2×1)) and dihydride (2H/Ge(100)−(1×1)) phases of atomic H adsorbed on Ge(100). The incident electron energy was 8 eV in both cases.

(1×1) periodicity, consistent with the generation of dihydride species due to breaking of the dimer bonds (the SiH_2 rocking mode at ∼490 cm^{-1} could not be resolved[35]). The slow transition and the broadness of the vibrational features suggest that the (1×1) phase is probably a mixture of mono-, di-, and possibly trihydride species.[36] Upon heating to 600 K, the scissor mode disappears and there is a shift in the frequency of the bending and stretching modes, indicating desorption of dihydride features and re-establishment of the monohydride phase, which then desorbs at 800 K. A pure monohydride phase can therefore be obtained by saturation above 600 K.[34] This phase exhibits an extremely sharp (2×1)−(1×2) LEED pattern, which confirms the general agreement that only this procedure leads to a pure monohydride phase.[43] Figure 1 shows HREEL spectra recorded for the dominant phases after saturating the surface with H either at room temperature, the dihydride or 2H/Si(100)−(1×1) phase, and at 600 K, the monohydride or 1H/Si(100)−(2×1) phase. A (3×1) phase could also be formed by exposure to ∼300 L of hydrogen,[35] but the resulting HREELS spectrum revealed no significant differences from the (1×1) phase.

For the Ge(100) surface, monohydride species are characterized by bending (ω(GeH)) and stretching (ν(GeH)) vibrations at 555 and 1990 cm^{-1}, respectively, while dihydride species show an additional scissor mode ($\delta(GeH_2)$) at 830 cm^{-1} (Figure

2). The dihydride surface (2H/Ge(100)−(1 × 1)) was prepared by exposure to 2000 L of hydrogen at room temperature, and the monohydride phase (1H/Ge(100)−(2 × 1)) required exposures of 500 L at 500 K. It was not possible to prepare a complete dihydride phase accompanied by a pure (1 × 1) LEED pattern, and even very high hydrogen exposures always revealed a weak 2-fold periodicity in the diffraction patterns.[37−39]

3.2. Dipole Scattering Theory. Experimental distinction between the different electron scattering mechanisms can be achieved by measuring the vibrational loss intensity as a function of incident electron beam energy, E_0, and scattering geometry. A theoretical treatment of dipole scattering is relatively straightforward, and for a well-ordered surface, Persson[26] showed that the differential cross section for inelastically scattered electrons at not too large angles away from specular is given by

$$\frac{d\sigma}{d\Omega} = \left(\frac{m\mu e}{\pi\epsilon_0\hbar^2}\right)^2 \sqrt{\frac{E_1}{E_0}} \frac{1}{\cos\alpha_i} \left(\frac{k_0 \sin\alpha_i - k_1 \sin\alpha_s}{{k_0}^2 + {k_1}^2 - 2k_0k_1\cos(\alpha_i - \alpha_s)}\right) \quad (1)$$

with m the electron mass, E_0 the incident electron energy, E_1 the energy of the inelastically scattered electrons ($E_1 = E_0 - h\nu$, where ν is the loss frequency), k_0 and k_1 the appropriate wavevectors, and α_i and α_s the angle of the incoming and outgoing electrons with respect to the surface normal. The dipole moment of the vibrational mode, μ, is expressed as a harmonic oscillator, i.e.,

$$\mu = q\sqrt{\frac{\hbar}{2M_r\omega}} \quad (2)$$

where M_r is the effective mass of the oscillator (here Si(Ge)−H), ω its angular frequency, and q (=dμ/dx) the dipole derivative or dynamic effective charge, which relates the dependence of the dipole moment on the internuclear distance x of the oscillator. The dynamic effective charge is generally unknown for adsorbate systems, and in the subsequent analysis, it is used as a variable to fit the theoretical values to the experimental observations.

The actual cross section σ is obtained by integrating over the solid angle of the scattered electrons that corresponds to the area detected by the spectrometer. The original derivation by Persson[26] assumed that the electrons were scattered into a circular cone of half angle, θ_{acc}, around the specularly reflected beam, i.e.,

$$\sigma = \left(\frac{\mu e}{\hbar\epsilon_0 v_0}\right)^2 \frac{1}{2\pi\cos\alpha_i}\left[(\sin^2\alpha_i - 2\cos^2\alpha_i)\frac{{\theta_{acc}}^2}{{\theta_{acc}}^2 + {\theta_0}^2} + (\sin^2\alpha_i + 2\cos^2\alpha_i)\ln\left(1 + \frac{{\theta_{acc}}^2}{{\theta_0}^2}\right)\right] \quad (3)$$

where v_0 is the velocity of the incident electrons and $\theta_0 = h\nu/2E_0$ is the width of the electrons inelastically scattered by dipole excitation of an adsorbate mode assuming $\theta_0 < \theta_{acc}$. However, the type of spectrometer used in these experiments involves cylindrical deflectors that focus only in the radial plane, and the detected cone is elliptical rather than circular. This was approximated by assuming a rectangular cone with variable acceptance angle, θ_{acc}, along this focusing plane and a constant azimuthal angle, θ_{az}. The differential cross section was considered to change only along the focusing plane and the scattering cross section requires integration along θ_{acc}, i.e.,

$$\sigma = \int_{\alpha_s-\theta_{acc}}^{\alpha_s+\theta_{acc}} \frac{d\sigma}{d\Omega}\theta_{az}\,d\theta_{acc} \quad (4)$$

It was found that for integration around the specular direction, the difference between eqs 3 and 4 was negligible, assuming a θ_{az} to match the detection area covered by a circular or elliptical cone, respectively. Equation 3 was therefore used for energy-dependent measurements that were always performed in specular geometry ($\alpha_i = \alpha_s$), while eq 4 was employed for angular dependent calculations, since this involved integration for off-specular geometries ($\alpha_i \neq \alpha_s$).

The angle of half acceptance, θ_{acc}, was determined experimentally by varying the angle of the incident electrons and estimating the angular deviation needed for the intensity of the scattered electrons to drop to half its magnitude at specular geometry. This procedure is displayed in Figure 3 for 2H/Si(100)−(1 × 1) using three different incident electron energies (E_0 = 1.5, 6, and 13 eV). The inset shows the general dependence of θ_{acc} on the incident electron energy for both 1H/Si(100)−(2 × 1) and 2H/Si(100)−(1 × 1). This figure clearly indicates a drastic increase of θ_{acc} for electron energies smaller than ∼5 eV. These electrons experience more diffuse scattering and larger momentum transfers, so a greater fraction of the electrons suffer large angle deflections. By contrast, θ_{acc} drops to a constant value of about 0.75° at higher electron energies. This is the actual instrumental width determined by measuring θ_{acc} for the spectrometer in the straight-through position.

The actual intensity of the loss peak relative to the specular elastic intensity, I_{loss}/I_0, which is the variable used for comparison with the experimental data, can then be determined from

$$\frac{I_{loss}}{I_0} = n_s\sigma \quad (5)$$

where n_s is the number of SiH (or GeH) species per surface area.

3.3. Excitation Functions for H/Si(100) and H/Ge(100). Specular HREEL spectra recorded for 1H/Si(100)−(2 × 1) at various incident electron energies are shown in Figure 4. The spectra are all normalized to an elastic intensity of 5 × 10^5 counts per second, and only the spectral regions associated with the bending ω(SiH) and stretching ν(SiH) modes are displayed. The intensity of ω(SiH) appears to increase steadily with decreasing energy, while the intensity of ν(SiH) fluctuates and exhibits clear maxima at 5.25 and 3.25 eV. The increase in background and the slight shift in the loss energy of ν(SiH) for the spectrum recorded at 1 eV might be explained by the experimental limitations of the spectrometer, since a loss energy of ∼250 meV represents a substantial fraction of the incident electron beam energy.

The normalized intensity of these modes is plotted in Figure 5 as a function of E_0. Also shown is the calculated intensity (dashed line) for dipole excitation using eqs 3 and 5, with a variable θ_{acc} based on Figure 3. The increasing intensity with decreasing E_0 can be explained by the extended time the electrons spend within the range of the oscillating electric field of the adsorbate, which enhances the possibility for energy transfer for vibrational excitation. The drastic reduction of intensity below approximately 2 eV is due to the sharper increase of θ_0 with respect to θ_{acc}, which means that the spectrometer does not detect the full dipole lobe of the backscattered electrons.

In the case of ω(SiH), the experimental intensity distribution is close to that expected for dipole excitation, although there is

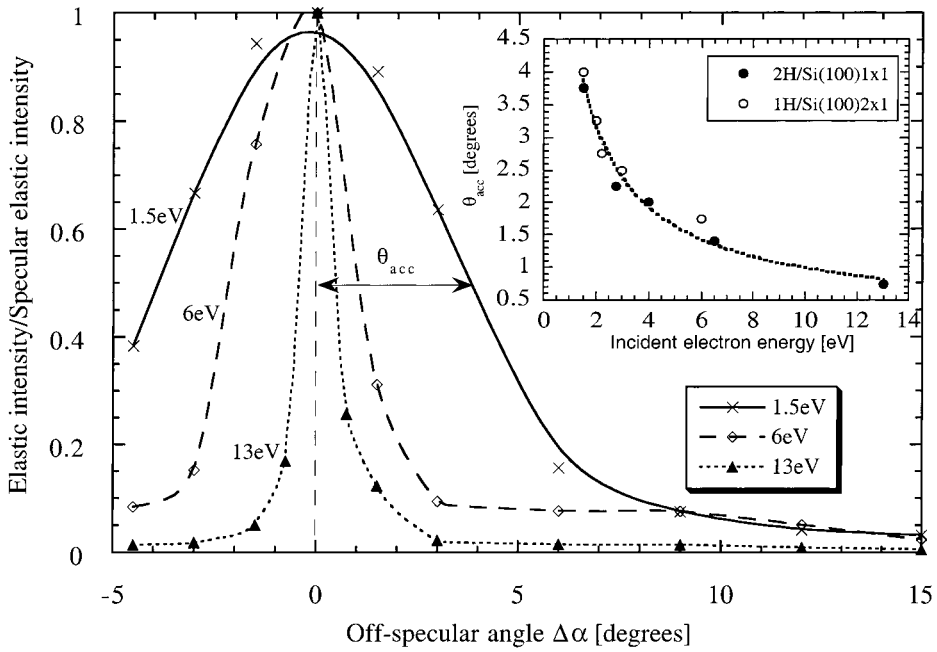

Figure 3. Dependence of the elastic beam intensity as a function of angular deviation, $\Delta\alpha$, away from the specular direction (specular at $\alpha_{i,s} = 45°$, $\Delta\alpha < 0$ indicates toward the surface normal) for three different incident electron beam energies for the dihydride phase on Si(100); the half angle of acceptance of the spectrometer, θ_{acc}, is indicated in the figure. The inset shows the resulting energy dependence of the half angle of acceptance for the monohydride and dihydride phases on Si(100).

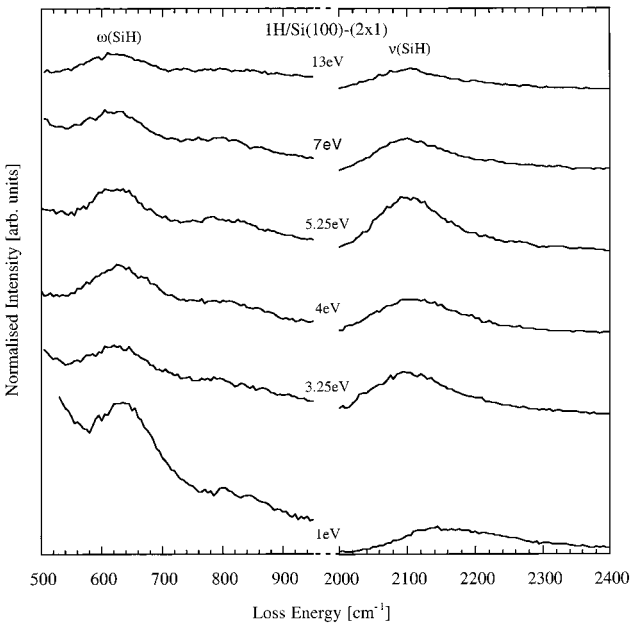

Figure 4. Normalized HREELS spectra at various electron beam energies for 1H/Si(100)−(2 × 1) in the spectral range corresponding to the bending (ω(SiH)) and stretching modes (ν(SiH)).

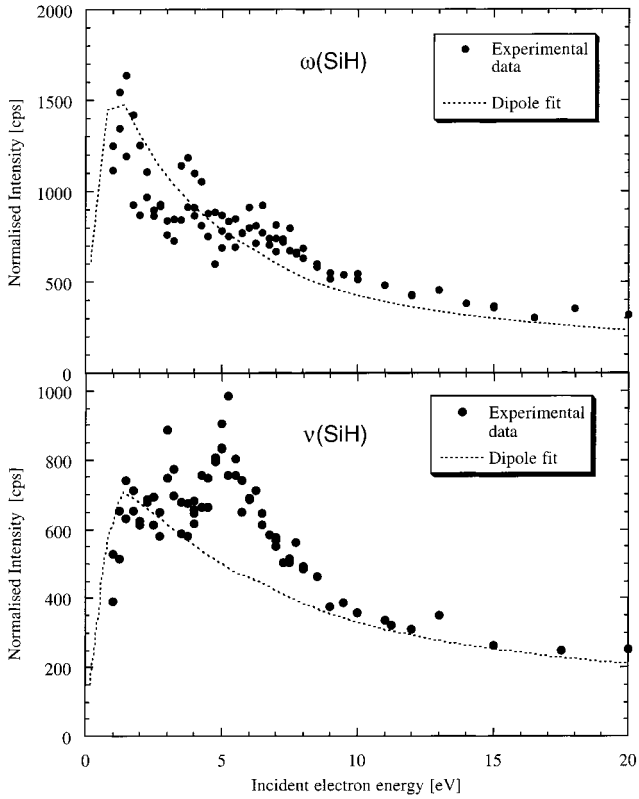

Figure 5. Normalized intensity of the bending (ω(SiH)) and stretching mode (ν(SiH) for 1H/Si(100)−(2 × 1) as a function of incident electron energy. The appropriate fit assuming dipole excitation (section 3.2) is shown by the dashed lines.

a slightly higher intensity at around 3.5−4 eV and at ∼5−6 eV. By contrast, ν(SiH) shows strong deviations from dipole scattering behavior between 3 and 8 eV, with clear maxima observed at about 3−3.5 eV and 5−5.5 eV. At all other energies, the fit to dipole scattering behavior is very good and the implication is that ν(SiH) is additionally excited by a nondipole mechanism at these two energies.

Similar measurements were carried out for 2H/Si(100)−(1 × 1), and the data is plotted in Figure 6 for the (a) $\omega(SiH_2)$, (b) $\delta(SiH_2)$, and (c) $\nu(SiH_2)$ vibrational modes. The intensity distributions for the first two follow dipole behavior except for the slight increase in intensity at ∼6 eV. The $\nu(SiH_2)$ mode however shows substantial enhancements between 2 and 7 eV, and a strong maximum is visible at 3−3.5 eV, with a slight shoulder at ∼6 eV. It is clear that the stretching vibrations for both the monohydride and dihydride phases are excited by a nondipole mechanism at certain low electron beam energies, but the mechanism of excitation is vibrational mode selective.

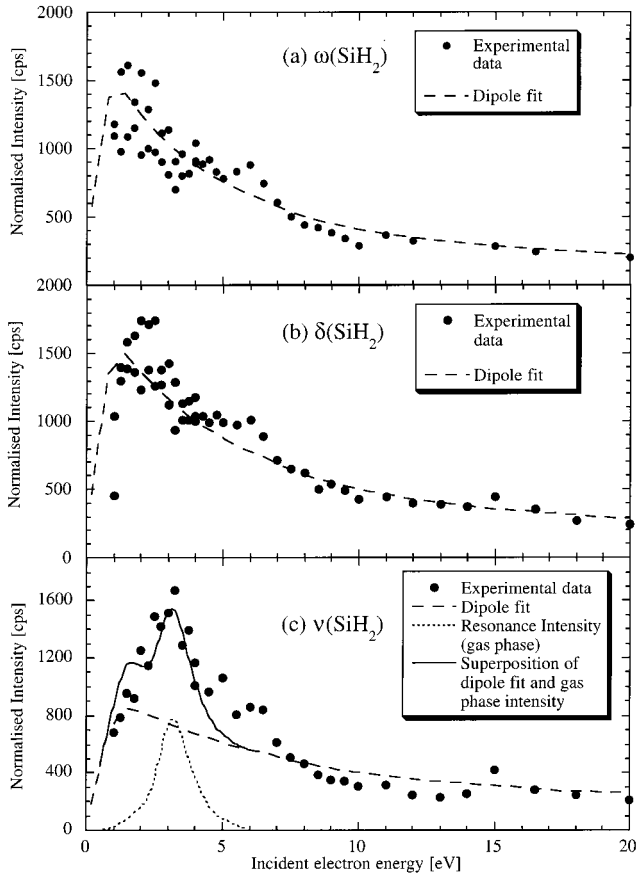

Figure 6. Normalized intensity of the (a) bending ($\omega(SiH_2)$), (b) scissor ($\delta(SiH_2)$), and (c) stretching ($\nu(SiH_2)$) modes for 2H/Si(100)−(1 × 1). The appropriate fit assuming dipole excitation is represented by the dashed lines. The intensity of the stretching mode for SiH_4 in the gas phase between 1 and 6 eV is also plotted as the dotted line in (c), its superposition onto the dipole fit being represented by the solid line.

Inelastic electron scattering studies of SiH_4[44,45] and Si_2H_6[46] in the gas phase have identified a broad shape resonance for the Si−H stretching mode at around 2 eV and this has been explained by the existence of a localized low-lying σ^* molecular orbital (MO). The gas-phase excitation function obtained for this mode for SiH_4 is plotted in Figure 6c,[44] although it should be noted that the maximum has been shifted up in energy by about 1 eV to coincide with that observed in the HREELS experiments for 2H/Si(100)−(1 × 1). (Andersson and Davenport[47] have related gas-phase cross sections to adsorbate loss functions by using the surface reflectivity. In our case, normalization has been performed by multiplying the gas-phase excitation function by an arbitary constant.) The solid line in the figure corresponds to the summation of this excitation function with the theoretical distribution for the adsorbate vibrational mode calculated from pure dipole scattering behavior. There is an excellent fit to the $\nu(SiH_2)$ excitation function obtained from the HREELS data, and we therefore assign the strong maximum observed at ∼3 eV for both 1H/Si(100)−(2 × 1) and 2H/Si(100)−(1 × 1) to a NIR. The σ^* MO is localized predominantly on the surface Si and adsorbed H atoms, and trapping of an electron into this orbital will therefore lead to repulsion along the Si−H bonds and resonant excitation of vibrational modes along this axis, i.e., the ν(SiH) and $\nu(SiH_2)$ stretching modes, respectively.

Further evidence for the NIR at 3 eV is provided by the data in Figure 7, which shows the dependence of the Si−H stretching

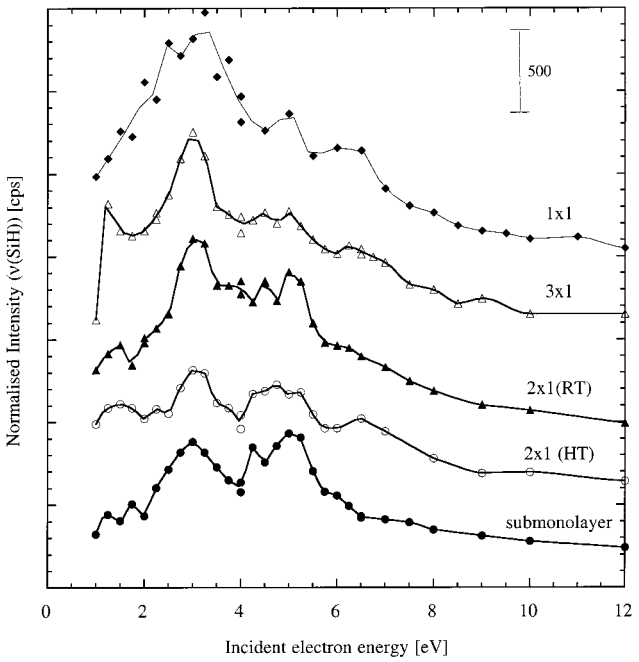

Figure 7. The normalized intensity of the stretching mode of hydrogen adsorbed on Si(100) for various adsorbate phases in order of increasing coverage as a function of incident electron beam energy.

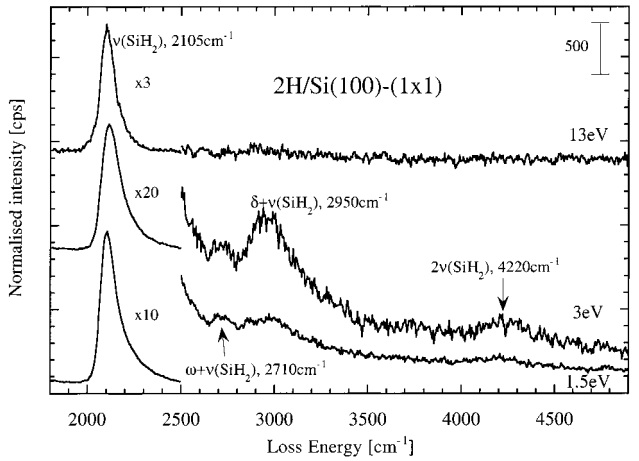

Figure 8. HREELS spectra of 2H/Si(100)−(1 × 1) in the range 1800−4800 cm^{-1} at three different incident electron beam energies.

mode intensity on E_0 for a variety of H coverages and phases. Excitation functions are shown for submonolayer coverage, where only a fraction of the dangling bonds of the clean surface are saturated with hydrogen, the pure monohydride phase formed after exposure at 600 K, the (2 × 1) phase formed by exposure at room temperature, the (3 × 1) phase which contains both monohydride and dihydride species, and the pure (1 × 1) dihydride phase. The plots are stacked in order of increasing hydrogen coverage, and each one shows a maximum at ∼3 eV in the intensity of the stretching mode which increases with coverage. Furthermore, the peak at ∼5 eV appears to decrease in intensity with increasing coverage, although it may simply be consumed by the increased intensity and width of the 3 eV maximum. The increase in the intensity of the 3 eV NIR simply reflects the increasing concentration of Si−H bonds present on the surface that can contribute to the NIR.

The enhanced intensity of overtones and combination bands is also a signature of a NIR.[10] Figure 8 displays the loss modes in the energy range 1800−4800 cm^{-1} for the dihydride phase on Si(100) at three different energies; 1.5, 3, and 13 eV. The

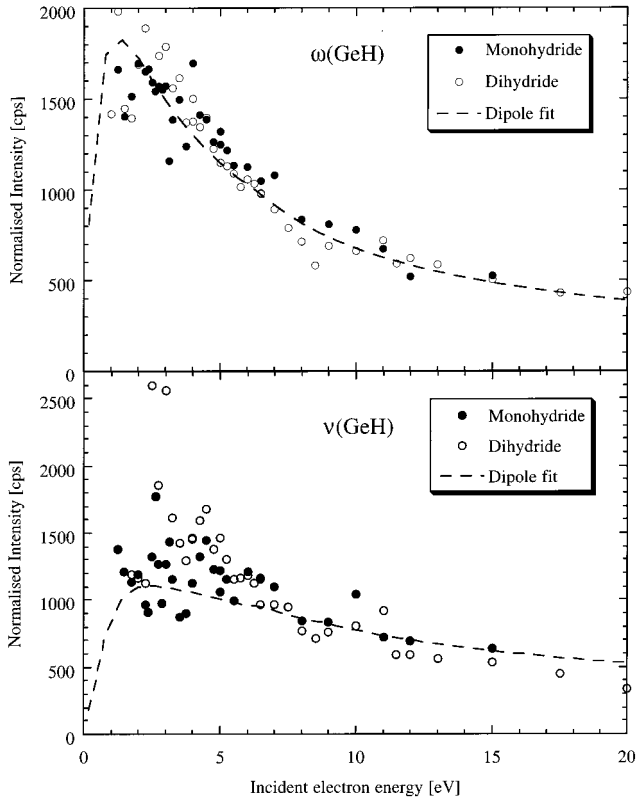

Figure 9. Normalized intensity of the bending (ω(GeH)) and stretching (ν(GeH)) modes for the monohydride and dihydride phases formed on Ge(100) as a function of incident electron energy. The experimental data is represented by open (dihydride) and closed (monohydride) circles, the appropriate fit assuming dipole excitation by the dashed lines.

fundamental stretching mode at 2105 cm^{-1} is clearly enhanced at 3 eV, while the intensity of several overtone and combination bands is also significantly greater at this energy, i.e., $2\nu(SiH_2)$ at 4220 cm^{-1}, $\omega(SiH_2) + \nu(SiH_2)$ at 2710 cm^{-1}, and $\delta(SiH_2) + \nu(SiH_2)$ at 2950 cm^{-1}. None of these features have any significant intensity in the spectra recorded at 1.5 and 13 eV.

The excitation functions plotted in Figures 5 and 6 for ν(SiH) and $\nu(SiH_2)$ suggest the presence of a second, higher energy maximum between 5 and 6 eV. This feature is also present in the excitation functions measured for the bending and scissor modes for both 1H/Si(100)$-(2 \times 1)$ and 2H/Si(100)$-(2 \times 1)$. Gas-phase electron scattering studies do not reveal a higher energy resonance, and its presence in the adsorbate excitation functions suggests it must be a substrate-related feature deriving either from a surface resonance or impact scattering. Previous HREELS studies for H/Si(111) and H/Si(100)[48−50] also indicated a peak in the excitation functions at ~6 eV, and this was tentatively assigned to a SR. Surface resonances generally exhibit dispersive behavior, and it is possible to monitor this by varying the specular scattering geometry for a fixed incident electron energy.[49,50] We carried out measurements at different geometries but found no conclusive evidence for strong dispersion of the 6 eV feature, although significant variations in intensity were observed for different specular geometries. We cannot therefore unambiguously assign this feature to a SR, and further detailed angular-dependent measurements and theoretical calculations are required to determine whether it arises from impact scattering or a surface resonance.

Similar measurements were carried out for the hydrogenated Ge(100) surface. Figure 9 shows the excitation functions for the ω(GeH) and ν(GeH) vibrational modes for both the monohydride and dihydride phases. The dashed lines again represent the theoretical calculation for each vibrational mode assuming pure dipole excitation. The ω(GeH) mode is excited preferentially by dipole scattering, and there is very little deviation in intensity from the calculated curve. By contrast, the ν(GeH) mode shows considerable deviation from dipole scattering behavior with a clear maxima at about 2.5 eV. The general interpretation is therefore similar to the hydrogenated Si(100) surface; both modes are excited predominantly by the dipole scattering mechanism, but there is also a contribution to the excitation of the stretching mode at specific beam energies from a nondipole interaction. Gas-phase electron scattering studies of germane indicated a NIR for the stretching mode at about 2−2.5 eV due to electron trapping in the lowest unoccupied molecular orbital of GeH_4.[51] We therefore assign the enhanced intensity in the HREELS measurements at 2.5−3 eV to a similar adsorbate based NIR.

4. Conclusions

The hydrogenated Si(100) and Ge(100) surfaces have been investigated by HREELS to gain more insight into the inelastic electron scattering mechanisms involved in the excitation of the bending, scissor, and stretching vibrational modes. All the studies were carried out on ordered adsorbate phases, and a clear distinction between dipole and nondipole excitation was possible through direct comparison between experimentally measured excitation functions and theoretical calculations based on pure dipole scattering behavior.

For the Si(100) surface, it was found that the bending and scissor modes for both the monohydride and dihydride phases are excited predominantly by dipolar excitation, but the stretching mode exhibits strong nondipole behavior between 2 and 6 eV. Through comparison with gas-phase electron scattering studies of silane and disilane, the maximum in the adsorbate excitation functions at ~ 3 eV is assigned to a negative ion resonance, in which the incident electrons are trapped in an antibonding σ^* orbital leading to enhanced vibrational excitation along the Si−H bond. A second maximum at ~5−6 eV could not be unambiguoulsy assigned and may be due to either a surface resonance or impact scattering.

Similar behavior was observed for the hydrogenated Ge(100) surface. Dipole scattering dominates the excitation functions for the bending and scissor modes, but the stretching mode is again enhanced between 2 and 6 eV, consistent with some nondipole behavior. Comparison with gas-phase studies of GeH_4 indicates that the observed maximum at 2.5−3 eV can again be assigned to a negative ion σ shape resonance.

It is clear that vibrational excitation of adsorbate modes in HREELS measurements on semiconductor surfaces is a complex process which may involve a number of different excitation mechanisms. Through an appropriate choice of the adsorbate system (in particular one that is well ordered), and by making careful comparison between experimentally determined excitation functions and theoretically derived vibrational loss cross sections, we have been able to distinguish dipole and nondipole behavior for atomic adsorbates even in specular scattering geometry. Furthermore, comparison between the measured excitation functions and those reported for related gas-phase molecules has allowed specific mode-selective negative ion resonances to be identified and assigned. It will be interesting to extend this work to more complex molecular adsorbates and systems for which well ordered phases are not formed.

Acknowledgment. This work was supported by the Engineering and Physical Sciences Research Council (EPSRC), U.K.

J. Eggeling thanks the German Academic Exchange Service (DAAD) for sponsorship of his Ph.D.

References and Notes

(1) Ibach, H.; Mills, D. L. *Electron Energy Loss Spectroscopy and Surface Vibrations*; Academic Press: New York, 1982.
(2) Chester, M. A.; Sheppard, N. In *Spectroscopy of Surfaces*; Clark, R. J. H., Hester, R. E., Eds.; John Wiley and Sons: New York, 1988; p 377.
(3) Gadzuk, J. W. In *Vibrational Spectroscopy of Molecules on Surfaces*; Yates, J. T., Jr.; Madey, T. E., Eds.; Plenum: New York, 1987; p 49.
(4) Erskine, J. L. *CRC Crit. Rev. Solid State Mater. Sci.* **1987**, *13*, 311.
(5) Tong, S. Y.; Li, C. H.; Mills, D. L. *Phys. Rev. Lett.* **1980**, *44*, 407.
(6) Tong, S. Y.; Li, C. H.; Mills, D. L. *Phys. Rev. B* **1981**, *24*, 806.
(7) Ho, W.; Willis, R. F.; Plummer, E. W. *Phys. Rev. Lett.* **1978**, *40*, 1463.
(8) DiNardo, N. J.; Demuth, J. E.; Avouris, Ph. *Phys. Rev. B* **1983**, *27*, 5832.
(9) Schulz, G. J. *Rev. Mod. Phys.* **1973**, *45*, 378, 423.
(10) Palmer, R. E.; Rous, P. J. *Rev. Mod. Phys.* **1992**, *64*, 383.
(11) Palmer, R. E. *Prog. Surf. Sci.* **1992**, *41*, 51.
(12) Palmer, R. E. *J. Electron. Spectrosc. Relat. Phenom.* **1993**, *64*/*65*, 39.
(13) Wong, S. F.; Schulz, G. J. *Phys. Rev. Lett.* **1975**, *35*, 1429.
(14) Rous, P. J.; Palmer, R. E.; Jensen, E. T. *Phys. Rev. B* **1990**, *41*, 4793.
(15) Aquino, A. A.; Jones, T. S. *Surf. Sci.* **1995**, *322*, 301.
(16) Mulcahy, C. P. A.; Aquino, A. A.; Rogers, J. J.; Jones, T. S. *J. Chem. Phys.* **1996**, *104*, 9120.
(17) Mulcahy, C. P. A.; Eggeling, J.; Jones, T. S. *J. Phys. Chem.* **1999**, *103*, 3187.
(18) Chen, Q.; Frederick, B. G.; Richardson, N. V. *J. Chem. Phys.* **1998**, *108*, 5942.
(19) Richardson, N. V.; Jones, T. S. *Appl. Phys. A* **1990**, *51*, 126. Richardson, N. V.; Jones, T. S. *Phys. Rev. Lett.* **1988**, *61*, 1752. Richardson, N. V.; Jones, T. S. *Surf. Sci.* **1989**, *211*/*212*, 377.
(20) Frederick, B. G.; Chen, Q.; Leibsle, F. M.; Lee, M. B.; Kitching, K. J.; Richardson, N. V. *Surf. Sci.* **1997**, *394*, 1.
(21) McRae, E. G. *Rev. Mod. Phys.* **1979**, *51*, 541.
(22) Conrad, H.; Scala, R.; Stenzel, W.; Unwin, R. *J. Chem. Phys.* **1984**, *81*, 6371.
(23) Conrad, H.; Kordisch, M. E.; Stenzel, W.; Sunjic, M.; Trninic-Radja, B. *Surf. Sci.* **1986**, *178*, 578
(24) Müssig, H. J.; Stenzel, W.; Song, Y.; Conrad, H. *Surf. Sci.* **1994**, *311*, 295.
(25) Jones, T. S.; Ashton, M. R.; Richardson, N. V. *J. Chem. Phys.* **1989**, *90*, 7564.
(26) Persson, B. N. J. *Solid State Commun.* **1977**, *24*, 573.
(27) Newns, D. M. *Phys. Lett.* **1977**, *60A*, 461.
(28) Andersson, S.; Persson, B. N. J.; Gustafsson, T.; Plummer, E. W. *Solid State Commun.* **1978**, *34*, 473.
(29) Andersson, S.; Persson, B. N. J. *Phys. Rev. Lett.* **1980**, *45*, 1421.
(30) Kolasinski, K. W. *Int. J. Mod. Phys. B* **1995**, *9*, 2753 and references within.
(31) Mönch, W. *Semiconductor Surfaces and Interfaces*; Springer-Verlag: Berlin, 1993 and references within.
(32) Schaefer, J. A.; Stucki, F.; Anderson, J. A.; Lapeyre, G. J.; Göpel, W. *Surf. Sci.* **1984**, *140*, 207.
(33) Stucki, F.; Schaefer, J. A.; Anderson, J. R.; Lapeyre, G. J.; Göpel, W. *Solid State Commun.* **1983**, *47*, 795.
(34) Butz, R.; Oellig, E. M.; Ibach, H.; Wagner, H. *Surf. Sci.* **1984**, *147*, 343.
(35) Angot, T.; Bolmont, D.; Koulmann, J. J. *Surf. Sci.* **1996**, 352−354, 401.
(36) Tautz, F. S.; Schaefer, J. A. *J. Appl. Phys.* **1998**, *84*, 6636.
(37) Papagno, L.; Shen, X. Y.; Anderson, J.; Schrripa Spagnolo, G.; Lapeyre, G. J. *Phys. Rev. B* **1986**, *34*, 7188.
(38) Chabal, Y. J. *Surf. Sci.* **1986**, *168*, 594.
(39) Gheyas, S. I.; Urisu, T.; Hirano, S.; Watanabe, H.; Iwata, S.; Aoyagi, M.; Nishio, M.; Ogawa, H. *Phys. Rev. B* **1998**, *58*, 9949.
(40) Ibach, H. *Electron Energy Loss Spectroscopy, the Technology of High Performance*; Springer Series in Optical Sciences, Vol. 63; Springer-Verlag: Berlin, 1991.
(41) Ibach, H.; Wagner, H.; Bruchmann, D. *Solid State Commun.* **1982**, *42*, 457.
(42) Papagno, L.; Caputi, L. S.; Frankel, D.; Chen, Y.; Lapeyre, G. J. *Surf. Sci.* **1987**, *189*/*190*, 199.
(43) Maruno, S.; Iwasaki, H.; Horioka, K.; Li, S.-T.; Nakamura, S. *Surf. Sci.* **1982**, *123*, 18.
(44) Tronc, M.; Hitchcock, A.; Edard, F. *J. Phys. B: At. Mol. Opt. Phys.* **1989**, *22*, L207.
(45) Tanaka, H.; Boesten, L.; Sato, H.; Kimura, M.; Dillon, M. A.; Spence, D. *J. Phys. B: At. Mol. Opt. Phys.* **1990**, *23*, 577.
(46) Dillon, M. A.; Boesten, L.; Tanaka, H.; Kimura, M.; Sato, H. *J. Phys. B: At. Mol. Opt. Phys.* **1994**, *27*, 1209.
(47) Andersson, S.; Davenport, J. W. *Solid State Commun.* **1978**, *28*, 677.
(48) Dumas, P.; Chabal, Y. J.; Jakob, P. *Surf. Sci.* **1992**, *269*/*270*, 867.
(49) Dumas, P.; Chabal, Y. J. *J. Vac. Sci. Technol. A* **1992**, *10*, 2160.
(50) He, Y.; Yu, L.-M.; Thiry, P. A.; Caudano, R. *Surf. Rev. Lett.* **1998**, *5*, 63.
(51) Dillon, M. A.; Boesten, L.; Tanaka, H.; Kimura, M.; Sato, H. *J. Phys. B: At. Mol. Opt. Phys.* **1993**, *26*, 3147.